1   **Title: Biomass burning emissions in north Australia during the early dry season:**

2   **an overview of the 2014 SAFIRED campaign**

3   **Authors:**

4   Marc D. Mallet[1], Maximilien J. Desservettaz[2], Branka Miljevic[1*], Andelija Milic[1],

5   Zoran D. Ristovski[1], Joel Alroe[1], Luke T. Cravigan[1], E. Rohan Jayaratne[1], Clare Paton-

6   Walsh[2], David W.T. Griffith[2], Stephen R. Wilson[2], Graham Kettlewell[2], Marcel V. van

7   der Schoot[3], Paul Selleck[3], Fabienne Reisen[3], Sarah J. Lawson[3], Jason Ward[3], James

8   Harnwell[3], Min Cheng[3], Rob W. Gillett[3], Suzie B. Molloy[3], Dean Howard[4], Peter F.

9   Nelson[4], Anthony L. Morrison[4], Grant C. Edwards[4], Alastair G. Williams[5], Scott D.

10   Chambers[5], Sylvester Werczynski[5], Leah R. Williams[6], V. Holly L. Winton[7,n], Brad

11   Atkinson[8], Xianyu Wang[9], Melita D. Keywood[3*]

12   **Affiliations:**

13   [1]Department of Chemistry, Physics and Mechanical Engineering, Queensland University of Technology,

14   Queensland, Brisbane, 4000, Australia

15   [2]Centre for Atmospheric Chemistry, University of Wollongong, Wollongong, New South Wales, 2522,

16   Australia

17   [3]CSIRO Oceans and Atmosphere, Aspendale, Victoria, 3195, Australia

18   [4]Department of Environmental Sciences, Macquarie University, Sydney, New South Wales, 2109,

19   Australia

20   [5]Australian Nuclei Science and Technology Organisation, Sydney, New South Wales, 2232, Australia

21   [6]Aerodyne Research, Inc., Billerica, Massachusetts, 01821, USA

22   [7]Physics and Astronomy, Curtin University, Perth, Western Australia, 6102, Australia

23   [8]Bureau of Meteorology, Darwin, Northern Territory, 0810, Australia

24   [9]National Research Centre for Environmental Toxicology, Brisbane, Queensland, 4108, Australia

25   [n]Now at the British Antarctic Survey, Cambridge, CB3 0ET, United Kingdom

26   ***Corresponding Authors:**

27   Dr Melita Keywood

28   Contact Phone: +613 9239 4596

29   Contact Email: melita.keywood@csiro.au

30

31   Dr Branka Miljevic

32   Contact Phone: +61 7 3138 3827
33
34   Contact Email: b.miljevic@qut.edu.au

Abstract

The SAFIRED (Savannah Fires in the Early Dry Season) campaign took place from 29th of May, 2014 until the 30th June, 2014 at the Australian Tropical Atmospheric Research Station (ATARS) in the Northern Territory, Australia. The purpose of this campaign was to investigate emissions from fires in the early dry season in northern Australia. Measurements were made of biomass burning aerosols, volatile organic compounds, polycyclic aromatic carbons, greenhouse gases, radon, speciated atmospheric mercury, and trace metals. Aspects of the biomass burning aerosol emissions investigated included; emission factors of various species, physical and chemical aerosol properties, aerosol aging, micronutrient supply to the ocean, nucleation, and aerosol water uptake. Over the course of the month-long campaign, biomass burning signals were prevalent and emissions from several large single burning events were observed at ATARS.

Biomass burning emissions dominated the gas and aerosol concentrations in this region. Dry season fires are extremely frequent and widespread across the northern region of Australia, which suggests that the measured aerosol and gaseous emissions at ATARS are likely representative of signals across the entire region of north Australia. Air mass forward trajectories show that these biomass burning emissions are carried north west over the Timor Sea and could influence the atmosphere over Indonesia and the tropical atmosphere over the Indian Ocean. Here we present characteristics of the biomass burning observed at the sampling site and provide an overview of the more specific outcomes of the SAFIRED campaign.

1. Introduction

Tropical north Australia is dominated by savannah ecosystems. This region consists of dense native and exotic grasslands and scattered trees and shrubs. Conditions are hot, humid and wet in the summer months of December through March with hot, dry conditions for the rest of the year giving rise to frequent fires between June and November each year. Human settlements are relatively scarce in northern Australia, outside of the territory capital, Darwin (population of 146 000). To the north of the continent are the tropical waters of the Timor Sea, as well as the highly populated Indonesian archipelago. South of the savannah grasslands are the Tanami, Simpson and Great Sandy Deserts, spanning hundreds of thousands of square kilometers. Emissions from fires in the savannah regions of northern Australia are therefore the most significant regional source of greenhouse and other trace gases, as well as atmospheric aerosol. Globally, savannah and grassland fires are the largest source of carbon emissions from biomass burning(van der Werf et al., 2010;Shi et al., 2015) and play a significant role in the earth's radiative budget. It is therefore important to quantify, characterise and fully understand the emissions from savannah fires in northern Australia, taking into account the complexity, variability and diversity of the species emitted.

In Australia approximately 550 000 km^2 of tropical and arid savannahs burn each year (Meyer et al., 2012;Russell-Smith et al., 2007), representing 7% of the continent's land area. In the tropical north of Australia, the fires during the early dry season in May/June consist of naturally occurring and accidental fires, as well as prescribed burns under strategic fire management practice to reduce the frequency and intensity of more extensive fires in the late dry season in October and November (Andersen et al., 2005).

85   These fires in the early dry season burn with a low to moderate intensity and are

86   normally confined to the grass-layer. Events where fires reach the canopy level are rare.

87   These prescribed burns are an important process for the region and are undertaken by

88   local landholders with permits, as well as government supported bodies and volunteers.

89   There has been a recent push to reinstate traditional Aboriginal fire management

90   regimes in this region (Russell-Smith et al., 2013). Other fire management regimes are

91   implemented in similar environments around the world, such as the savannah

92   ecosystems of Africa (Govender et al., 2006) or the chaparral grasses in the United

93   States (Akagi et al., 2012). In general, fire management regimes are considered to

94   benefit regional biodiversity and can lead to the long-term increase in living biomass,

95   resulting in a reduction of greenhouse gas emissions (Russell-Smith et al., 2013).

96   Quantifying the emissions from dry season fires on regional scales is essential for

97   understanding the impact of these fires on the local and global atmosphere.

98

99   The components and concentrations of emissions from savannah fires are dependent

100   upon the vegetation and burning conditions. While CO_2 is the primary product of

101   biomass burning (BB), combustion processes also result in the emission of many other

102   trace gases such as CO, CH_4, NOx, N_2O as well as non methane organic compounds

103   (NMOCs) and aerosol particles composed of elemental carbon, organic carbon and

104   some inorganic material (Crutzen and Andreae, 1990). The state of organics in biomass

105   burning aerosols can vary significantly due to the type of plant material burned, the

106   characteristics of the fires themselves as well as through aging processes in the

107   atmosphere.

108

109   The effects of these emissions on radiative forcing are complex. The global average

110   radiative forcing due to biomass burning aerosol-radiation interaction is estimated in

111   the 5th International Panel on Climate Change report as 0.0 W m^{-2} with an uncertainty

112   range of -0.20 to +0.20 Wm^{-2} (Bindoff et al., 2013). It is well known that greenhouse

113   gases have a positive radiative forcing, heating up the atmosphere. Light absorbing

114   carbon in the aerosol phase will also result in a positive radiative forcing (Jacobson,

115   2001) by absorbing shortwave radiation. Conversely, the presence of aerosol organic

116   and inorganic matter can result in a negative radiative forcing by scattering solar

117   radiation (Penner et al., 1998). In addition, biomass burning has been shown to be a

118   significant source of cloud condensation nuclei (CCN), despite typically being

119   composed of weakly hygroscopic substances (Lawson et al., 2015), due to the high

120   number of particles emitted. This can result in a change in cloud droplet concentrations

121   and volume, thereby influencing cloud formation, albedo and lifetime. The contribution

122   of each species to the overall radiative forcing is also likely to change as smoke plumes

123   age (Liousse et al., 1995). Furthermore, not all biomass burning aerosol will interact

124   with radiation in the same way. For example, fresh BB emissions in the tropics has been

125   observed to be more absorbing than those from boreal forest fires(Wong and Li, 2002).

126   The role of biomass burning emissions is not limited to the Earth's radiative budget.

127   Certain species of emissions (e.g., mercury) can be deposited and sequestered in soil

128   (Gustin et al., 2008), vegetation (Rea et al., 2002) or bodies of water (LaRoche and

129   Breitbarth, 2005).

130

131   Large-scale studies in Africa (Keil and Haywood, 2003), North America (Yokelson et

132   al., 2009;Singh et al., 2006), Europe (Saarikoski et al., 2007), South America (Ferek et

133   al., 1998) and Asia (Lin et al., 2013;Du et al., 2011) have provided valuable insight into

134 the impact of fire emissions on the regional atmosphere and laboratory measurements

135 have proved to be useful in understanding the emission factors, composition and

136 atmospheric processing of these emissions (Stockwell et al., 2014). Despite this, there

137 is still a need for a better scientific understanding of the influence biomass burning has

138 on atmospheric composition and air quality (Kaiser and Keywood, 2015), particularly

139 around Australia. Furthermore, the tropics are disproportionately under-sampled and

140 the atmospheric and ocean processes in these regions are of both regional and global

141 consequence. The SAFIRED campaign will contribute towards better understanding

142 biomass burning emissions and the atmospheric composition in tropical Australia.

143

144 On a more specific level, the SAFIRED campaign was undertaken with the following

145 objectives:

146 • To obtain Australian savannah fire dry season emission factors for greenhouse

147   gases, polycyclicaromatic hydrocarbons, gaseous elemental mercury, non-

148   methane organic compounds, Aitken and accumulation mode aerosols and non-

149   refractory submicron organic, sulfates, ammonia, nitrates and chlorides.

150 • To understand the emission of mercury from north Australian fires and to

151   quantify the delivery of mercury to the ecosystem.

152 • To characterise the composition and size of aerosols in the region of north

153   Australia and to understand the influence and extent of biomass burning on the

154   total aerosol burden.

155 • To assess the ability of biomass burning aerosol to act as cloud condensation

156   nuclei and to establish a link between aerosol composition, size and CCN.

157   •   To assess the fractional solubility of aerosol iron and other trace metals in this

158   region in the context of the potential supply of micronutrients required for

159   marine primary production in the ocean.

160   2. Description of experiment

161   **2.1 Site**

162   The Australian Tropical Atmospheric Research Station (ATARS; 12°14'56.6"S,

163   131°02'40.8"E) is located on the Gunn Point peninsula in northern Australia (see Figure

164   1). ATARS is operated by the Australian Bureau of Meteorology and the CSIRO

165   (Commonwealth Scientific and Industrial Research Organisation). Standard

166   meteorological measurements (wind velocity, atmospheric pressure, precipitation) run

167   permanently at ATARS and two laboratories are in place for the installation of other

168   instruments. The SAFIRED campaign took place from 29th May 2014 until the 30th

169   June 2014, with personnel and instruments from nine institutes utilising these

170   laboratories to make comprehensive gaseous and aerosol measurements during this

171   period of the early dry season.

172   **2.2 Instruments and measurements**

Table 1 A summary of the quantities measured during SAFIRED and the respective instrument or measurement technique. Detection limits and uncertainties are expressed for select instruments or measurements.

Quantity	Instrument or Technique	Sample frequency	Reference	Detection limits	Uncertainties
CO, CO_2, CH_4 and N_2O	Fourier transform infrared spectrometry	3 minute	(Griffith et al., 2012)	0.04 mg CO_2 $m^{-2}s^{-1}$, 20 ngN $m^{-2}s^{-1}$ (N_2O), 30 ng CH_4 $m^{-2}s^{-1}$)	0.02 (CO_2), 0.2 (CH_4), 0.1 (N_2O), 0.2 (CO) [a]
O_3	UV Photometric Ozone Analysis	1 minute		0.50 ppb	~1 ppb
Non methane organic compounds	Proton Transfer-Mass Spectrometry, high performance liquid chromatography of Supelco cartridge samples; gas chromatography of adsorbant tubes	3 minute; 12 hour; 12 hour	(Galbally et al., 2007); (Cheng et al., 2016); (Lawson et al., 2015, Dunne et al. (2017))	2 - 563 ppt (PTR-MS ions)	<22% (PTR-MS ions)
Polycyclic aromatic hydrocarbons (gas and particle phase)	Gas chromatography and high resolution mass spectrometry of filter and foam samples	24 hour	(Wang et al., 2017)	<1 pg m^{-3}	<±20% (rep)
Gaseous elemental mercury; gaseous oxidised mercury; and particulate-bound mercury	Cold vapour atomic fluorescence spectroscopy	5 minute; 2 hour; 2 hour	(Landis et al., 2002); (Steffen et al., 2008)	0.1 ng m^{-3} (GEM), 2 pg m^{-3} (GOM), 2 pg m^{-3} (PBM)	N.R. [b]
Radon	700L dual-flow two filter detector	1 hour	(Chambers et al., 2014)	±0.04 Bq m^{-3}	10 - 14%
Aerosol mobility size distributions (14 nm to 670 nm); neutral and charged aerosol size distributions (0.8 nm to 42 nm)	Scanning mobility particle sizer, Neutral cluster and air ion spectrometry	5 minute; 4 minute	(Mirme et al., 2007)	-	±1% in size selection, ±10% in CPC counts
Cloud condensation nuclei concentration (at 0.5% supersaturation)	Supersaturated streamwise continuous-flow of aerosols in a wetted column using thermal-gradient followed by Optical Particle Counting of activated CCN	10 second	(Gras et al., 2007)	-	±0.1% SS, ±20% in OPC counts
Elemental and organic carbon; water soluble ions; and anhydrous sugars (PM_1 and PM_{10})	β+ attenuation; ion chromatography; high performance anion-exchange chromatography	12 hour	(Chow et al., 2007b); (Iinuma et al., 2009)	0.0009 µg m^{-3} (oxalate), 0.0002 µg m^{-3} (levoglucosan)	N.R.
Soluble and total fraction of trace metals (PM_{10})	High-resolution inductively coupled plasma mass spectrometry analysis of extracted leachates and digests.	24 hour	(Winton et al., 2016)	< 1 pg m^{-3}	±5% in soluble Fe, ±3% in total Fe
Non-refractory chemical composition (PM_1)	Time-of-flight aerosol mass spectrometry	3 minute	(Drewnick et al., 2005)	0.003 µg m^{-3} (NO_3^-, SO_4^{2-}), 0.03 µg m^{-3} (NH_4^+, organics)	~±20%
Aerosol volatility and hygroscopicity (50 nm and 150 nm)	Volatility and hygroscopicity tandem differential mobility analysis	12 minute (full cycle)	(Johnson et al., 2004)	-	±1% in size sselection, ±1% in RH, ±3% in thermodenuder temperature

ᵃ Uncertainty expressed as measurement precision (Allan deviation) for one minute, expressed in μmol mol^{-1}

ᵇ To be discussed in future work

176

2.2.1 Trace Gases

Greenhouse gases

Continuous measurement of CO_2, CO, CH_4 and N_2O were made using a high precision FTIR trace gas and isotope Spectronus analyser, developed by the Centre for Atmospheric Chemistry at the University of Wollongong. The analyser combines a Fourier Transform Infrared (FTIR) Spectrometer (Bruker IRcube), a pressure and temperature controlled multi-pass cell and an electronically cooled mercury cadmium telluride detector. A detailed description of the instrument and concentration retrieval technique are available in Griffith et al. (2012) and Griffith (1996).

Ozone and other trace gases

A Multi Axis Differential Optical Absorption Spectrometer (MAX-DOAS) was installed on the top of one of the laboratories during the campaign. The technique has been shown to provide the vertical profile of nitrogen dioxide, ozone, sulfur dioxide, formaldehyde, glyoxal and aerosol extinction (Sinreich et al., 2005;Honninger et al., 2004). The MAX-DOAS instrument used in this campaign was designed and built at the University of Wollongong. It consists of a vertically rotating prism capturing scattered solar radiation at different angles (1°, 2°, 4°, 8°, 16°, 30° and a reference at 90°) into a fibre optic that carries the radiation to a UV-Visible spectrometer (AvaSpec – ULS3648). Furthermore, a Thermo Scientific model 49i UV Photometric Ozone analyser was used to measure ozone concentrations. Several periods of elevated biomass burning emissions resulted in interferences with the 49i UV analyser and were removed from the analyses. These periods were marked with strong correlations with

199 high concentrations of acetonitrile where other UV-absorbing species, such as certain

200 PAH species.

201 **Non-methane organic compounds**

202 Online NMOC measurements were made using a high sensitivity Proton Transfer

203 Reaction-Mass Spectrometer (PTR-MS; Ionicon Analytik) using H_3O^+ as the primary

204 ion. The inlet was 10 m in length and drew air at 5 L min^{-1} from 2 m above the roof

205 (approx 5.5 m above ground level). The PTR-MS ran with inlet and drift tube

206 temperature of 60 ºC, 600 V drift tube, and 2.2 mbar drift tube pressure, which equates

207 to an energy field of 135 Td. The PTR-MS sequentially scanned masses 15-190, with

208 1 second dwell time. The PTR-MS operated with the aid of auxiliary equipment which

209 regulates the flow of air in the sample inlet and controls whether the PTR-MS is

210 sampling ambient or zero air or calibration gas (Galbally et al., 2007).

211

212 Furthermore, AT VOC (adsorbent tube Volatile Organic Compounds) samples were

213 collected by an automatic VOC sequencer which actively draws air through two multi-

214 adsorbent tubes in series (Markes Carbograph 1TD / Carbopack X). The adsorbent

215 tubes were then analysed by a PerkinElmer TurboMatrix™ 650 ATD (Automated

216 Thermal Desorber) and a Hewlett Packard 6890A gas chromatography (GC) equipped

217 with a Flame Ionization Detector (FID) and a Mass Selective Detector (MSD) at CSIRO

218 Oceans and Atmosphere laboratories. Further details of the sampling and analyses are

219 given in Cheng et al. (2016).

220

221 During sampling, carbonyls and dicarbonyls were trapped on S10 Supelco cartridges,

222 containing high-purity silica adsorbent coated with 2,4-dinitrophenylhydrazine

223 (DPNH), where they were converted to the hydrazone derivatives. Samples were

224 refrigerated immediately after sampling until analysis. The derivatives were extracted

225 from the cartridge in 2.5 mL of acetonitrile and analysed by high performance liquid

226 chromatography with diode array detection. The diode array detection enables the

227 absorption spectra of each peak to be determined. The difference in the spectra

228 highlights which peaks in the chromatograms are mono- or dicarbonyl DNPH

229 derivatives and, along with retention times, allows the identification of the dicarbonyls

230 glyoxal and methylglyoxal. Further details can be found in Lawson et al. (2015).

231 **PAHs**

232 PAHs were sampled through a high-volume air sampler (Kimoto Electric Co., LTD.)

233 using a sampling rate typically at $\sim$60 m^{-3} h^{-1}. The sampling rate was calibrated using

234 an orifice plate prior to the sampling campaign and the sampling volume was calculated

235 based on the calibrated sampling rate and sampling duration. A bypass gas meter

236 installed on the sampler was used to monitor any anomalous fluctuation of the sampling

237 rate during the sampling period. Particle-associated and gaseous PAHs were collected

238 on glass fibre filters (Whatman™, 203×254 mm, grade GF/A in sheets) and subsequent

239 polyurethane foam plugs respectively. The glass fibre filters and polyurethane foam,

240 along with the field blank samples, were extracted separately using an Accelerated

241 Solvent Extractor (Thermo Scientific™ Dionex™ ASE™ 350) after being spiked with

242 a solution containing 7 deuterated PAHs (i.e. $^2D_{10}$-phenanthrene, $^2D_{10}$-fluoranthene,

243 $^2D_{12}$-chrysene, $^2D_{12}$-benzo[b]fluoranthene, $^2D_{12}$-BaP, $^2D_{12}$-indeno[1,2,3-cd]pyrene,

244 $^2D_{12}$-benzo[g,h,i]perylene) at different levels as internal standards for quantification

245 purposes. Concentrated extracts were cleaned up by neutral alumina and neutral silica.

246 Eluents were carefully evaporated to near dryness and refilled with 250 pg of $^{13}C_{12}$-

247 PCB (polychlorinated biphenyl) 141 (in 25 µL isooctane) employed as the

248 recovery/instrument standard for estimating the recoveries of the spiked internal

249 standards and monitoring the performance of the analytical instrument. Samples were

250 analysed using a Thermo Scientific™ TRACE™ 1310 gas chromatograph coupled to

251 a Thermo Scientific™ double-focusing system™ Magnetic Sector high resolution mass

252 spectrometer. The HRMS was operated in electron impact-multiple ion detection mode

253 and resolution was set to $\geq 10,000$ (10% valley definition). An isotopic dilution method

254 was used to quantify 13 PAH analytes including phenanthrene, anthracene,

255 fluoranthene, pyrene, benzo[a]anthrancene, chrysene, benzo[b]fluoranthene,

256 benzo[k]fluoranthene, benzo[e]pyrene, BaP, indeno[1,2,3-cd]pyrene,

257 dibenzo[a,h]anthracene, benzo[g,h,i]perylene.

258 **Mercury**

259 Total gaseous mercury, gaseous elemental mercury + gaseous oxidised mercury (TGM;

260 GEM + GOM), was sampled from a 10 m mast and measured via gold pre-concentration

261 and cold vapour atomic fluorescence spectroscopy using a Tekran 2537X instrument.

262 Simultaneously, GEM, GOM and Particulate-bound mercury (PBM) were individually

263 measured using a Tekran 2537B connected to a combined Tekran 1130/1135 speciation

264 unit sampling at a 5.4 m height. The sampling train of the 1130/1135 collects first GOM

265 (KCl-coated denuder) then PBM (quartz wool pyrolyser) in series from a 10 L min^{-1}

266 sampling flow, allowing GEM only to flow onwards for detection by subsampling by

267 the 2537B. Due to the small atmospheric concentrations of GOM and PBM, pre-

268 concentration occurred over a 1-hour period with subsequent analysis taking an

269 additional hour. Continuous measurements of GEM at 5-minute resolution were made

270 possible for the 2537B unit by rotating pre-concentration/analysis roles of the two

271 internal gold traps. Both 2537 units sampled at 1 L min^{-1} and were calibrated every 23

272 hours using an internal mercury permeation source. For more information on the 2537

273 and 1130/1135 systems see Landis et al. (2002) and Steffen et al. (2008).

274

275   GEM fluxes were measured using the methods outlined in Edwards et al. (2005). Air

276   samples were drawn at heights of 5.2 and 8.0 m through 46.4 m of nylon tubing using

277   a PTFE diaphragm pump operating at 10 L min^{-1}. Subsampling from this flow through

278   a 0.2 μm PTFE filter at 1 L min^{-1} by a Tekran 2537A, and switching between sample

279   intakes, allowed resolution of a GEM gradient every 30 minutes. The transfer velocity

280   was measured using a Campbell Scientific CSAT3 sonic anemometer and LI-COR

281   7200 closed path infrared gas analyser for CO_2, both located on the same tower as the

282   gradient intakes at 6.6 m and sampling at 20 Hz.

283   Radon

284   In order to measure Radon concentrations, a 700 L dual-flow-loop two-filter radon

285   detector, designed and built by the Australian Nuclear Science and Technology

286   Organisation (Whittlestone and Zahorowski, 1998;Chambers et al., 2014), was installed

287   at the ATARS in 2011 and has been fully operational since July 2012. The detector

288   provided continuous hourly radon concentrations for the duration of the SAFIRED

289   campaign, sampling air at 40 L min^{-1} from 12 m above ground level through 25 mm

290   high-density polyethylene agricultural pipe. A coarse aerosol filter and dehumidifier

291   were installed "upstream" of the detector, as well as a 400 L delay volume to ensure

292   that thoron (^{220}Rn, half-life 55 s) concentrations in the inlet air stream were reduced to

293   less than 0.5 % of their ambient values. The detector's response time is around 45

294   minutes, and the lower limit of detection is 40 - 50 mBq m^{-3}. Calibrations are performed

295   on a monthly basis by injecting radon from a PYLON 101.15±4% kBq Ra-226 source

296   (12.745 Bq min^{-1} ^{222}Rn), traceable to NIST standards, and instrumental background is

297   checked every 3 months. In post processing, half-hourly raw counts were integrated to

298   hourly values before calibration to activity concentrations (Bq m^{-3}).

2.2.2 Aerosols

Aerosol Drying System

An Automated Regenerating Aerosol Diffusion Dryer (ARADD) is permanently installed on the roof of the laboratory containing the aerosol instrumentation for this campaign. This was used in front of the aerosol manifold to continuously dry the aerosol sample. The ARADD design, similar to that described by Tuch et al. (2009), continuously conditions the aerosol sample to a relative humidity of below 40% with maximum aerosol transmission efficiency. The ARADD utilizes two diffusion drying columns in parallel, each containing 7 stainless steel mesh tubes of 10 mm internal diameter and approximately 800 mm length, surrounded by a cavity packed with silica gel. The aerosol sampled is directed into one column at a time, while the other column is regenerated by an ultra-dry compressed air system. All flows are controlled by software that directs sample flow and compressed air flow to the appropriate column with a series of valves. The ARADD has total suspended particulate style intake at the inlet of the aerosol sample path. This is a non-size-selective stainless-steel inlet with a semi-cicular hat over an inverted conical funnel of variable pitch ending with a 3/4" stainless-steel tube. In practise, the aerosols collected have an equivalent aerodynamic diameter of 100 μm or less depending on sampling conditions. The inlet led to a sample manifold at the exit of the system to provide sampling take-offs for the various aerosol instruments connected to the ARADD. Flow through the ARADD is provided by the instruments and pumps connected downstream. The ambient and inlet relative humidity for the entire sampling period were logged and are displayed in Supplementary Figure S1.

16

Aerosol Size

Aerosol size distributions were measured with a Scanning Mobility Particle Sizer (SMPS). A TSI 3071 long-column electrostatic classifier with a TSI 3772 Condensation Particle Counter (CPC) measured the size distribution over a range of 14 nm to 670 nm at a scan interval of 5 minutes.

In addition to the aerosol size distributions measured by the SMPS, neutral and charged aerosol particle distributions from 0.8 nm to 42 nm were measured using a Neutral cluster and Air Ion Spectrometer (NAIS)(Manninen et al., 2009;Mirme et al., 2007). In this study, the NAIS was set to operate in a cycle of 4 min including ion and neutral particle sampling periods of 2 and 1 minute, respectively, with the remaining minute being an offset period which is required to neutralize and relax the electrodes. The total sampling air flow was 60 L min^{-1}, the high flow rate being used to minimize ion diffusion losses and maximize the measured ion concentration sensitivity. Ion losses are accounted for during post-processing of the data by the software (Mirme et al., 2007).

Aerosol Composition and Water Uptake

PM_1 and PM_{10} 12-hour filter samples (night and day) were collected on a TAPI 602 Beta plus particle measurement system (BAM). Portions of the PM_1 filters have been analysed for elemental and organic carbon mass loadings using a DRI Model 2001A Thermal-Optical Carbon Analyzer following the IMPROVE-A temperature protocol (Chow et al., 2007b). Additional portions of the PM_1 filters were extracted in 5 ml of 18.2 mΩ de-ionized water and preserved using 1% chloroform. These extracts have been analysed for major water-soluble ions by suppressed ion chromatography and for

346 anhydrous sugars including levoglucosan by high-performance anion-exchange

347 chromatography with pulsed amperometric detection (Iinuma et al., 2009).

348

349 Daily aerosol filters were collected using two Ecotech 3000 high-volume volumetric

350 flow controlled aerosol samplers with PM$_{10}$ size selective inlets. One high-volume

351 sampler was used to collect aerosols on acid cleaned Whatman 41 filters to determine

352 the soluble and total fraction of trace metals. Soluble trace metals were extracted from

353 a filter aliquot using ultra-pure water (>18.2 mΩ) leaching experiments. Total trace

354 metal concentrations were determined by digesting a second filter aliquot with

355 concentrated nitric and hydrofluoric acids. Leachates and digested solutions were

356 analysed by high resolution inductively couple plasma mass spectrometry. The second

357 sampler was used to collect a set of aerosol samples on quartz filters for elemental and

358 organic carbon analysis following (Chow et al., 2007a), and major anion and cation

359 analysis.

360

361 The volatility and hygroscopicity of 50 nm and 150 nm particles were measured with a

362 custom built Volatility and Hygroscopicity Tandem Differential Mobility Analyser

363 (VH-TDMA). Inlet dried particles were size selected (alternating between 50 and 150

364 nm) using a TSI 3080 electrostatic classifier. Scans alternated between two different

365 sample pathways. In the first, after size selection, particles were passed through a

366 thermodenuder set to 120°C. The sample line was then split so that half went to an

367 SMPS comprised of a TSI 3080 classifier and a TSI 3010 CPC (V-TDMA). The rest of

368 the sample was passed through a humidifying system that exposed the particles to a

369 relative humidity of 90% before being brought into another SMPS with a 3080 classifier

370 and 3010 CPC (H-TDMA). Alternatively, the thermodenuder was bypassed in every

371 second scan so that the V-TDMA was used to verify the size selection and the H-TDMA

372 was able to observe the hygroscopic growth of ambient particles. Each scan ran for 3

373 minutes, giving a full set of data every 12 minutes.

374

375 The chemical composition and properties of non-refractory sub-micron particles were

376 investigated with a compact Time-of-Flight Aerosol Mass Spectrometer (cToF-AMS,

377 Aerodyne Research, Inc.) and a Time of Flight Aerosol Chemical Speciation Monitor

378 (ToF-ACSM, Aerodyne Research, Inc.). Both of these instruments operate with the

379 same principle and have many identical components. An aerodynamic lens in the inlet

380 of each instrument focuses the particles into a beam and differential pumping removes

381 most of the gas phase. Particles are flash vaporized at 600°C and ionized by electron

382 impact before passing through a time-of-flight mass spectrometer to a multi-channel

383 plate detector in the cToF-AMS and a dynode detector in the ToF-ACSM. The cToF-

384 AMS has the added benefit of having a particle Time-of-Flight (pToF) mode, which

385 allows the size resolved chemical composition to be measured. Both instruments

386 sampled through a $PM_{2.5}$ inlet and nafion dryer. In addition, the inlet of the cToF-AMS

387 was incorporated into the VH-TDMA system, so that when the VH-TDMA was

388 measuring ambient particles, the cToF-AMS would draw particles through the

389 thermodenuder set at 120°C and vice-versa. This gives additional information about the

390 chemical composition of the volatile component of submicron particles.

391

392 The number of particles activated to cloud droplets were measured using a Continuous-

393 Flow Steam Wise Thermal Gradient Cloud Condensation Nuclei Counter (CCNC) from

394 Droplet Measurement Technologies Inc. (DMT, model No. 100). Particles were

395   exposed to a 0.5% supersaturation and activated particles greater than 1µm were

396   counted with an Optical Particle Counter using a 50 mW, 658 nm laser diode.

397   **Back trajectories**

398   Hourly 10-day air mass back trajectories terminating at ATARS were produced using

399   the NOAA HYSPLIT model (Draxler and Rolph, 2003), and catalogued in a data base

400   for use with the SAFIRED campaign data set. Global Data Assimilation System input

401   files with 0.5° resolution were obtained from NOAA ARL FTP site

402   (http://ready.arl.noaa.gov/gdas1.php) to drive the HYSPLIT model.

403   **Satellite detection of fires**

404   Data on the location of fires was collected from the Australian national bushfire

405   monitoring system, Sentinel Hotspots. Hotspot locations are derived from the Moderate

406   Resolution Imaging Spectroradiometer (MODIS) sensors on the Terra and Aqua

407   satellites and the Visible Infrared Imaging Radiometer Suite (VIIRS) sensor on the

408   Suomi NPP satellite. The Terra, Aqua and Suomi NPP satellites fly over the region

409   around ATARS at approximately 10:30 am, 3 pm and 2:30 pm, respectively. Detection

410   of fires is therefore limited to those that are flaming during these times.

3. Overview of Campaign

Fires and air masses
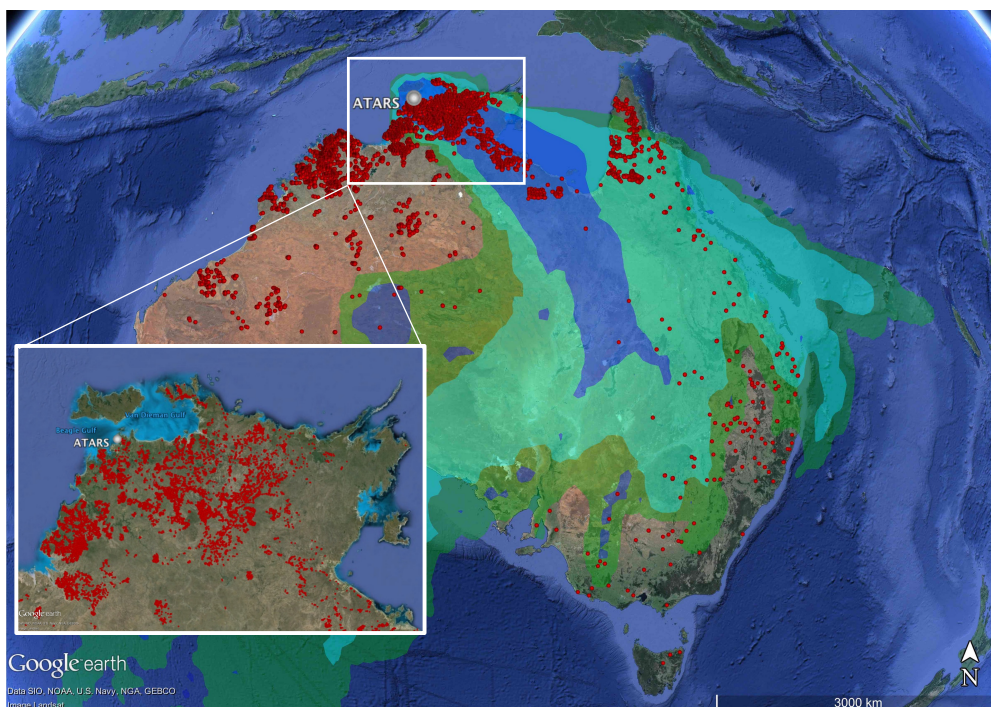
Figure 1 All satellite-detected fires with >50% detection confidence in June 2014 in Australia. Trajectory densities are shown as shaded regions (blue - >10% of all data; cyan - >1% of all data; green - >0.1% of all data)

Thousands of fires were observed in during the period of the SAFIRED campaign in Australia by the MODIS and VIIRS sensors on the Terra and Aqua NASA satellites. The vast majority of these occurred in the savannah regions of northern Australia. Over 28000 fires were detected within 400 km of ATARS during the sampling period. . Airmass back trajectories from the sampling site show that air masses over the study period predominately originated from the southeast (see Figure 1), generally over the regions where fires were frequently detected. Considering the daily satellite observations of close and distant fires, as well as meteorological, gaseous and aerosol measurements over the duration of SAFIRED, five periods were distinguished; four biomass burning related periods (BBP1, BBP2, BBP3 and BBP4) and a "coastal" period (CP). The dates for these periods are displayed in Table 2.

428　Table 2 The start and end dates for the four identified Biomass Burning Periods (BBP1, BBP2, BBP3 and
429　BBP4) and the Coastal Period (CP).

| Period	Start date (mm/dd/yy hh:mm)	End date (mm/dd/yy hh:mm)
BBP1	05/30/14 00:00	05/31/14 23:59
BBP2	06/06/14 00:00	06/12/14 23:59
BBP3	06/14/14 00:00	06/17/14 23:59
CP	06/19/14 12:00	06/22/14 23:59
BBP4	06/23/14 00:00	06/28/14 23:59

430

431　The number of detected fires on each day within 10 km, 20 km, 50 km, 100 km and 200

432　km of the sampling location was determined (see Figure 2). Several fires within 10 km

433　were detected on the 30th of May (BBP1), the 9th and 10th of June (BBP2) and the

434　25th and 26th of June (BBP4). BBP1, BBP2 and BBP4 were also associated with the

435　highest concentrations of most of the measured gaseous (Figure 3) and aerosol species

436　(Figure 4). The periods between the 12th and 23rd of June (BBP3 and CP) had very

437　few detected fires within 50 km of the station, corresponding to smaller gaseous and
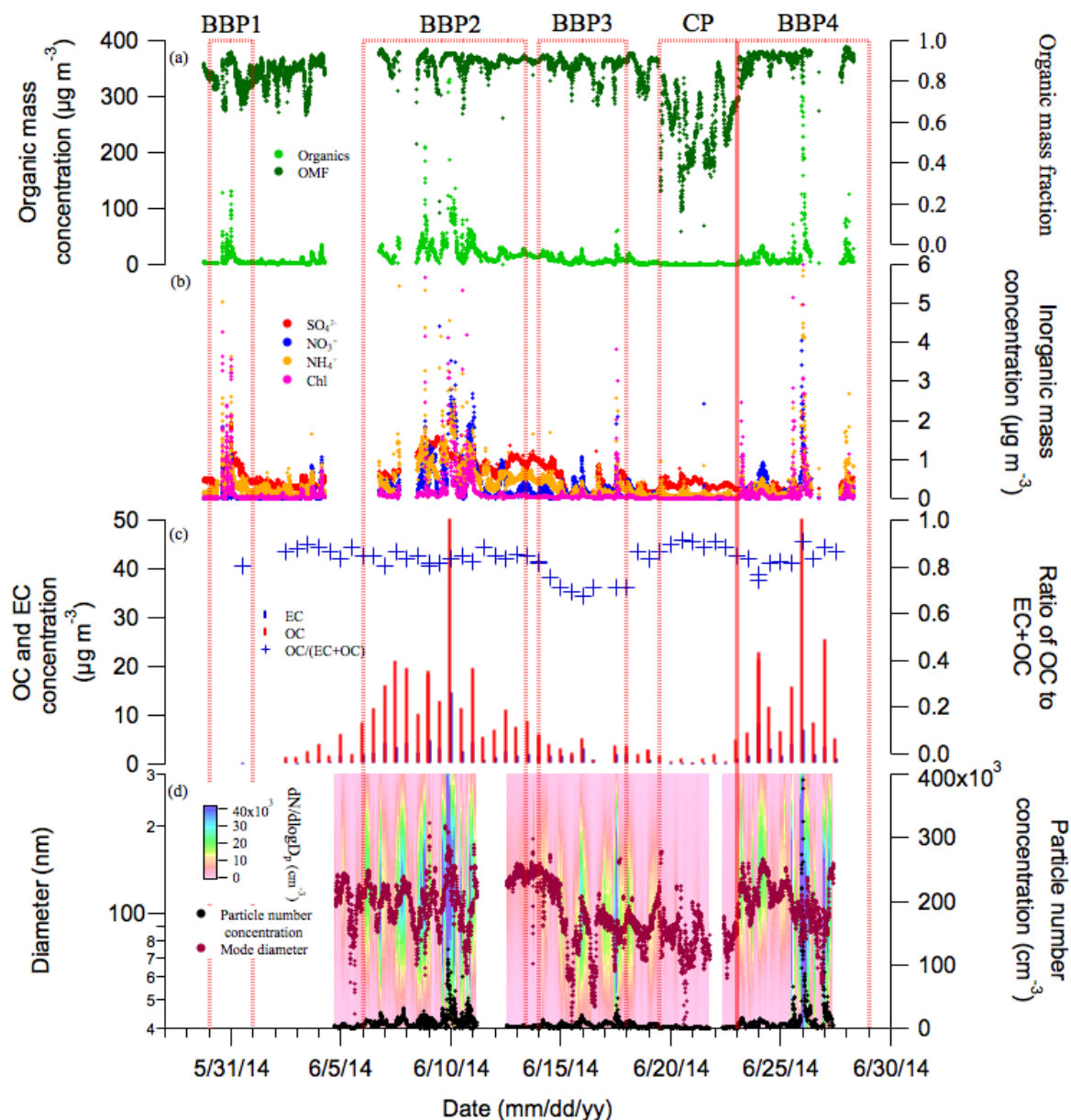
438　aerosol concentrations.

439

440
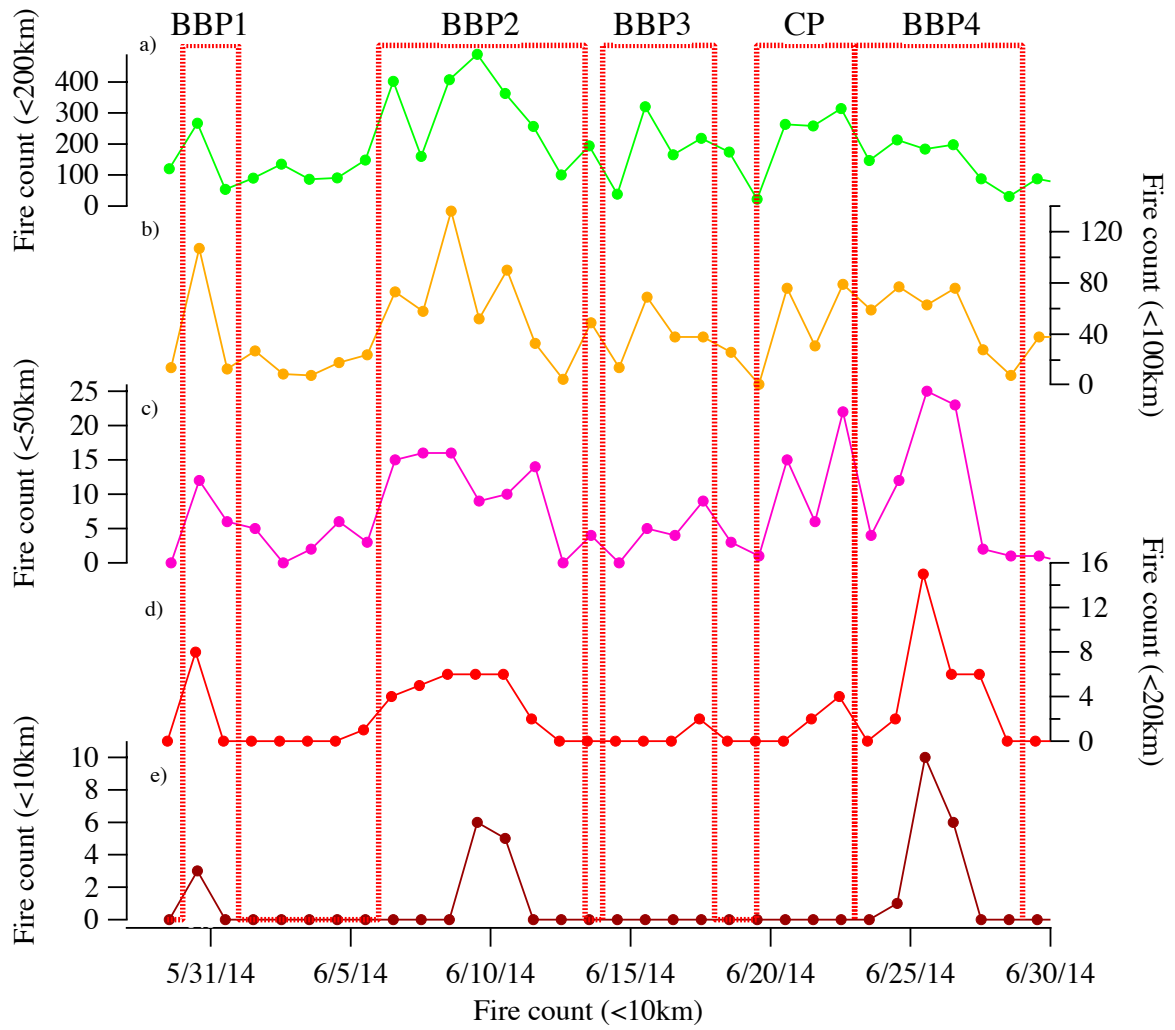
Figure 2 The number of hotspots observed each day within (a) 200 km, (b) 100 km, (c) 50 km, (d) 20 km and (e) 10 km of the ATARS, as detected by the MODIS and VIIRS sensors on the Terra and Aqua satellites.

443
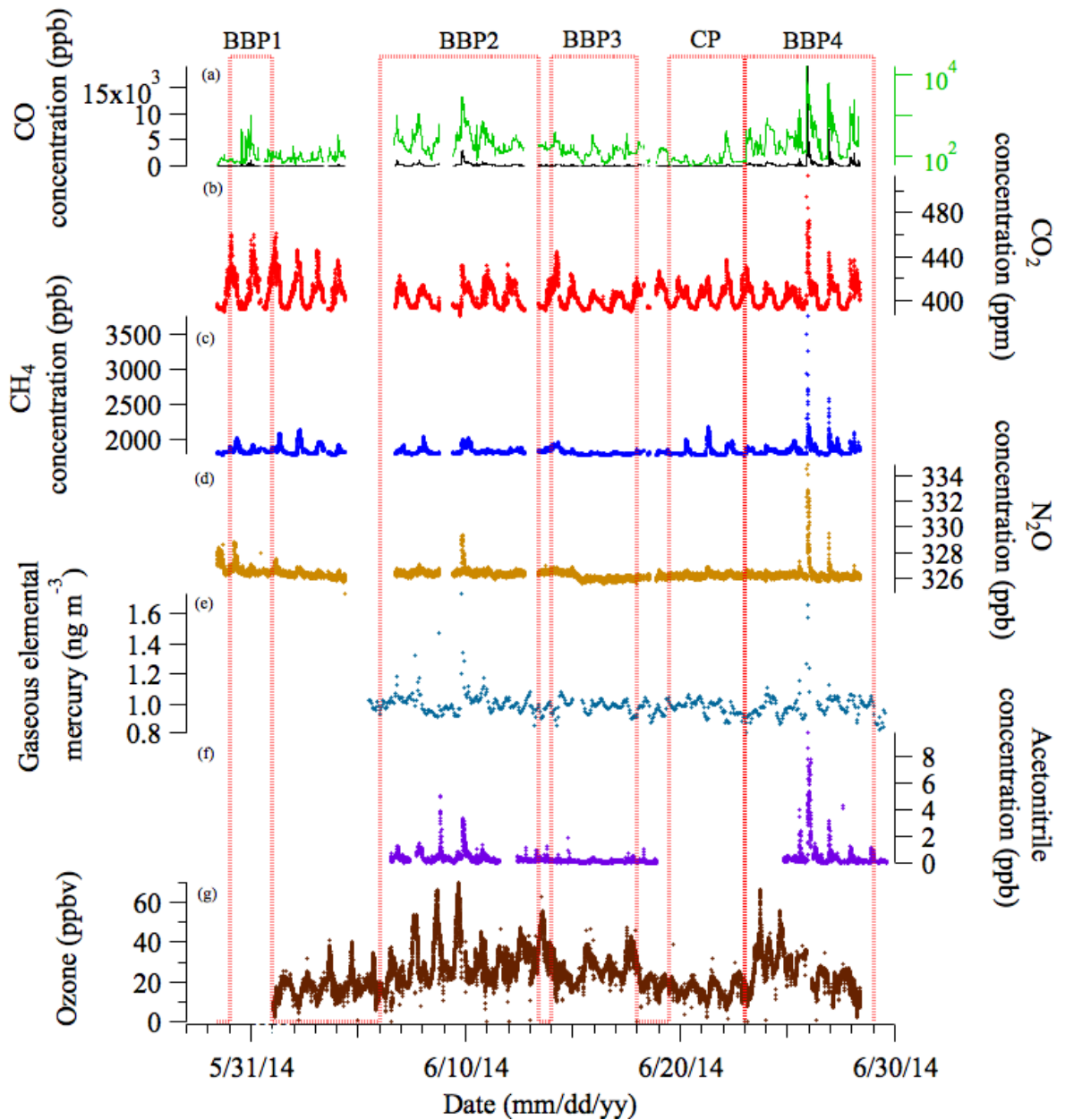
Figure 3 The time series of the major measured gaseous species during the SAFIRED campaign: (a) carbon
monoxide, (b) carbon dioxide, (c) methane, (d) nitrous oxide, (e) gaseous elemental mercury, (f) acetonitrile
and (g) ozone. The biomass burning and coastal periods are indicated by the red dotted lines. All parts-per
notation refer to mole fractions unless otherwise indicated. The date and time is local time.

Figure 4 The times series of the major aerosol properties during the SAFIRED campaign: (a) the non-refractory PM₁ organic mass concentration (left) and organic mass fraction (right), b) the inorganic non-refractory PM₁ mass concentrations, (c) the 12-hour filter OC and EC PM₁ mass concentrations (left) and the ratio of OC to OC+EC (right), (d) the particle size distributions and particle size mode (left) and the total particle number concentration (right) and (e) the wind direction at ATARS. The date and time is local time.

Most of the gaseous and aerosol time series show a pronounced diurnal trend, with higher concentrations typically observed during the night (see Figure 5 and Supplementary Figure and S2). This is likely due to a combination of variations in fire locations, time of burns, and changes in the boundary layer height or wind velocity. The diurnals trends of radon concentrations, temperature, wind speed, wind direction and greenhouse gases for each of the BBPs and the CP are displayed in Figure 5. The

25

460   radon concentrations provide further information regarding the regional air mass

461   origins and the degree of contact with the land surface and give insight into the

462   boundary layer. Sharp decreases in the radon concentrations were observed after 09:00

463   local time and did not increase until after sunset at approximately 18:00 for all periods

464   (Figure 5a), suggesting a pronounced diurnal variation in the boundary layer height.

465   Furthermore, radon concentrations were consistently lower during the CP than the BB

466   periods, suggesting less terrestrial influence than the rest of the sampling period. The

467   HYSPLIT air mass back trajectory for the CP originated along the east coast of

468   Australia and passing over little land before arriving at the station. Figure 5d supports

469   this, showing predominately easterly and northeasterly winds during the night and day,

470   respectively. The diurnal variations during the BB periods were more pronounced. The

471   winds during these periods were predominately southeasterly during the night and

472   morning, turning easterly during the afternoon before reverting at approximately 20:00

473   local time. The HYSPLIT air mass back trajectories for the BB periods indicated

474   terrestrial origins, with air masses passing predominately over the savannah region of

475   northern Australia where the fires occurred.
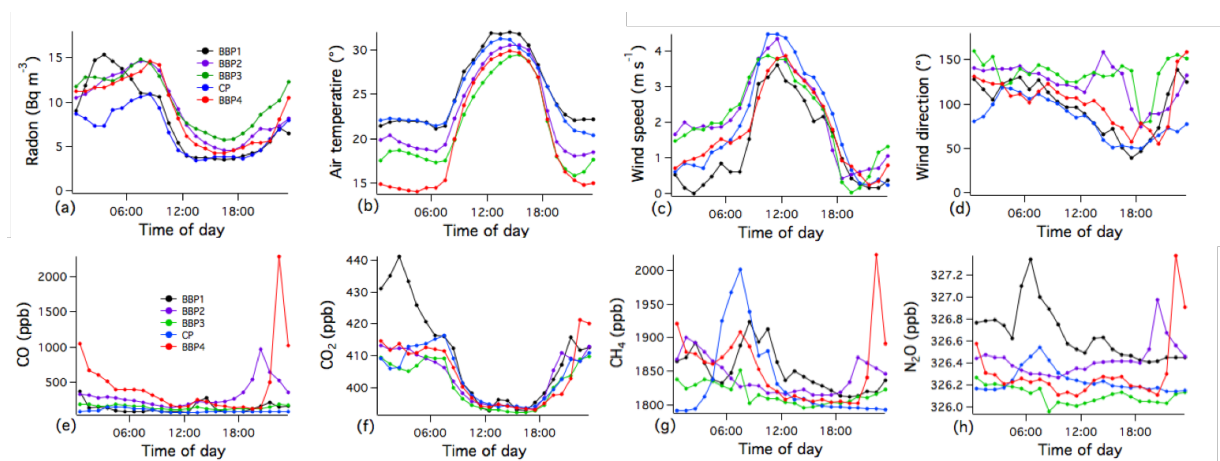

Figure 5 Mean hourly diurnal (a) radon, (b) wind speed, (c) wind direction (d) dew point temperature (e) CO, (c) CO_2, (d) CH_4, and (e) N_2O at ATARS, separated into different biomass burning periods (BBP) and a coastal period (CP)

26

480   With numerous fires occurring across the region and the limitations of once-per-day

481   satellite fly-overs and stationary measurements, it can be difficult to identify the exact

482   source of these elevated signals. Nonetheless, it is possible to link detected plumes with

483   fires given back trajectory analysis. The elevated signals during BBP1 were likely a

484   result of several fires that were burning and observed on the 30th of May at 14:00 local

485   time approximately 2 and 10 km from ATARS during the day. While the elevated

486   signals were observed later in the evening, it is likely that they were due to a

487   continuation or evolution of those fires. Some of the most intense signals of the

488   campaign were observed during BBP2, with numerous close (within 50 km) and distant

489   (within 200 km) detected. Due to the limitations of the once-per-day satellite fly-by, it

490   was only possible to link one of the observed plumes to a source during this period. A

491   large event observed on the evening of the 9th of June was likely due to a cluster of

492   fires detected approximately 5 km southeast of ATARS. Only one fire within 20 km of

493   ATARS was observed via satellite during BBP3 on the 17th of June but this was not

494   associated with any significant increase in gaseous or aerosol concentrations. Several

495   fires were also observed between 20 km and 50 km from the station. One close fire was

496   also observed during CP, however wind directions during this period were typically

497   north-easterly and concentrations were therefore much lower. 5-day HYSPLIT

498   trajectories also show that air mass during the CP originated along the east coast of

499   Australia before travelling towards the sampling station with very little terrestrial

500   influence.

501

502   For a portion of BBP4, fires were burning within several kilometers of ATARS and

503   several plumes were easily observed from the station. The signals from these plumes

504   are shown in Figure 6. The observed enhancements between 12:30 and 15:00 pm on

505   the 25th June during BBP4 were a result of grass fires burning approximately 2 km

506   south-east from the station. During this event, the wind direction was highly variable,

507   changing between 140° and 80° True Bearing (TB) multiple times. As a result, the

508   sampling changed from measuring the air mass with and without the plume from this

509   fire, which led to sharp increases and decreases in biomass burning-related signals.

510   Visually, the fire area and extent of the plume was larger at 4:00pm than earlier,

511   however the wind direction changed to north-easterly which directed the plume away

512   from the station. From 16:00 until 22:00, the wind direction was stable at

513   approximately 50° TB. At 22:00, the wind direction rapidly changed to directly south

514   and the largest enhancements for the whole campaign were observed until

515   approximately 2:00 am on the 26th of June. It is very likely that these signals were a

516   result of a continuation and evolution of these fires as the night progressed. Portions of

517   a ~0.25 km^2 grassland field within 500 m directly south of ATARS were observed to

518   be burned upon arrival at the station on the morning of the 26th of June and we speculate

519   that the burning of this field contributed to the large enhancements in measured biomass

520   burning emissions. The emissions during this portion of BBP4 are likely to be the most

521   representative of fresh biomass burning smoke during the SAFIRED campaign.

522   Significant ozone enhancements over 80 ppb were observed during this event, although

523   this was likely result of a cross-contamination due to concurrently high concentrations

524   of UV-absorbing organic compounds in the gaseous phase. This enhancement would

525   only be possible with significant photochemical processing which is very unlikely

526   considering the time of the event, the visual evidence of close fires, and the large

527   concentrations observed.
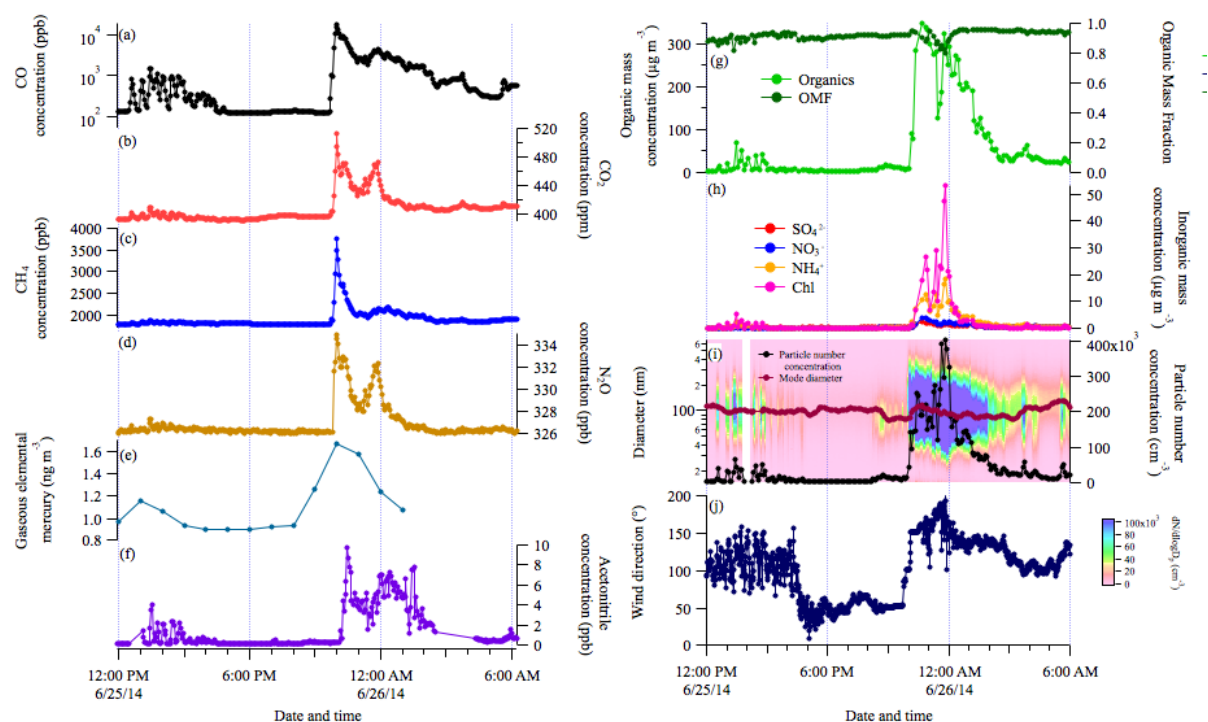
Figure 6 The major gas and aerosol concentrations measured during two biomass burning events within 1 km of ATARS during BBP4. (a) through (g) and (h) through (k) are as per Figures 3 and 4, respectively. All parts-per notation or mole fractions unless otherwise indicated. The date and time are local time.

Based on the elevated concentrations of biomass burning related gaseous and aerosol species, detection of close fires and the air mass back trajectory analysis during portions of BBP1, BBP2 and BBP4, these periods are likely associated with fresh biomass burning smoke from nearby fires. With smaller concentrations and more distant observed fires, the signals observed during BBP3 are possibly more characteristic of aged biomass burning smoke. The influence of biomass burning during CP was much smaller than the rest of the campaign. Investigating the relationship between toluene and acetonitrile, two NMOCs emitted from biomass burning, can provide further information on the aging of BB emissions. Toluene is much shorter lived than acetonitrile as it readily reacts in the presence of the OH radical. Assuming a consistent emission ratio of these two NMOCs from fires in this region, the ratio of toluene/acetonitrile thereby provides a proxy for photochemical age. Unfortunately, the PTR-MS which measures these species was not operational during BBP1 and CP. The

545   diurnal trends for the toluene and acetonitrile concentrations and the

546   toluene/acetonitrile ratio is shown in Figure 7 for BBP2, BBP3 and BBP4. The

547   toluene/acetonitrile ratio was highest during the night, indicating more photochemically

548   aged smoke throughout the day. Interestingly, while the toluene and acetonitrile

549   concentrations were consistently higher during BBP2 and BBP4 than BBP3, the

550   toluene/acetonitrile ratio was of the same magnitude and followed the same trend. It is

551   therefore plausible that, while there were not large enhancements in concentrations

552   during BBP3 and there were few fires detected close-by during the daytime satellite

553   flyovers, there were small-scale burns during the night that were close enough for the

554   emissions to reach sampling site. This observation highlights the limitation of using

555   satellite hotspot detection in fully understanding the aging processes of biomass

556   burning emissions.
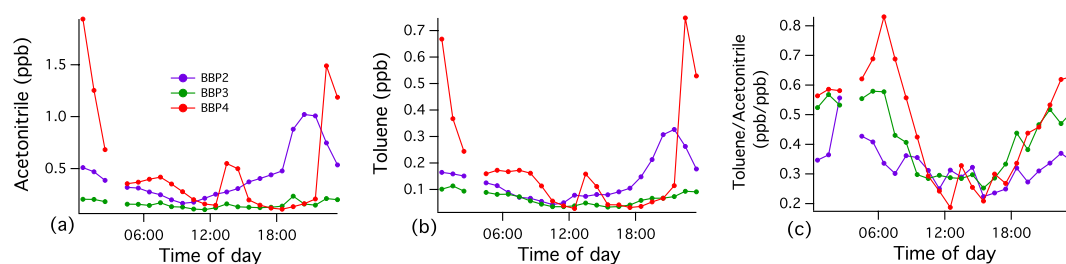
557

558 **Figure 7** **Mean hourly diurnal (a) acetonitrile concentration, (b) toluene concentration, (c) toluene/acetonitrile**
559 **ratio, separated into different biomass burning periods (BBP).**

560

561   Particle size distributions were unimodal for the majority of the sampling period with

562   a mode of approximately 100 nm on average (see Figure 8). The SMPS was not

563   operational during BBP1. Although the shape of the BBP4 size distribution was similar

564   to the campaign average, concentrations were much higher and a result of close fires.

565   BBP2 had a slightly larger size distribution centered on 110 nm. The size distribution

566   during BBP3 was slightly smaller than the campaign average and BBP2 and BBP4,

567   with a mode centered on ~95 nm. Furthermore, the diurnal trends of the BBA mode

568   diameter during BBP2, BBP3 and BBP4 and CP all showed a clear maximum during

569   the night (see Supplementary Figure S2d). The diurnal trends of the toluene/acetonitrile

570   ratios (Figure 7c) as well as the ratio of oxygenated organic aerosol to total organics

571   (see Supplementary Figure S2c) suggest that the larger night time particle sizes are

572   more associated with fresh biomass burning. The contrast between these size

573   distributions could be a result of atmospheric aging and dilution in which organic mass

574   condenses onto or evaporates from the particle. Variations in fuel load or burning

575   conditions could also contribute to this difference. The size and concentration of

576   particles during the Coastal Period (CP) were much smaller than the rest of the

577   campaign. There were two periods during CP where a bimodal size distribution was

578   observed; one from approximately 3 pm until midnight on the 19th of June and the other

579   between 2 pm and 6 pm on the 20th of June. The size distributions for both of these

580   periods had a mode at approximately 20 nm and another at approximately 85 nm.

581   Submicron sulfates made up to 32% of the total submicron non-refractory mass

582   concentrations, as reported by the cToF-AMS from the period of midday on the 19th of

583   June until midnight on the 22nd of June, whereas the average sulfate contribution for

584   the rest of the campaign was approximately 8%. The low radon values, small particle

585   concentrations, bimodal size distributions and significant contributions of sulfate

586   during this period also suggest very little biomass burning signal and a more marine-

587   like aerosol. No particle nucleation events were observed over the entire sampling

588   period (See Supplementary Figure S3). This is likely due to the elevated particle

589   concentrations acting as a condensation sink.

592

593
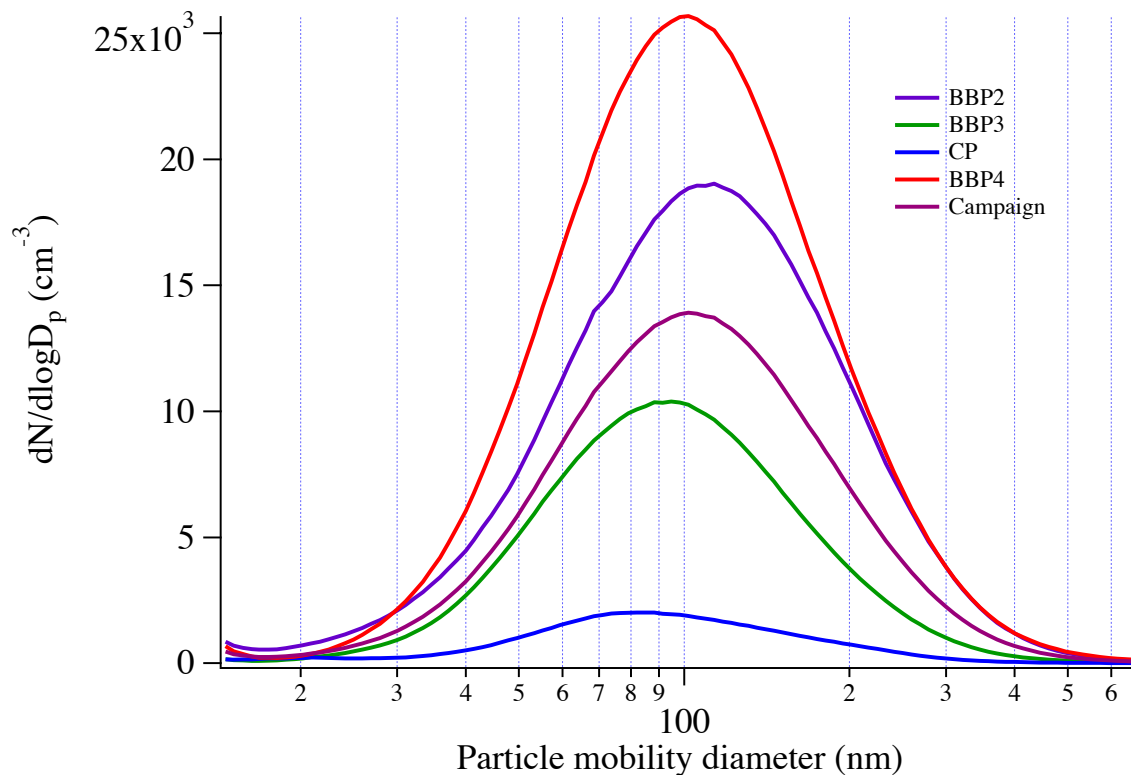
Figure 8 The average number size distribution during BBP2, BBP3, BBP4, CP and the campaign average.

Over the campaign, organics dominated the non-refectory sub-micron aerosol mass

contributing, on average, 90% of the total mass. Sulphate, nitrates, ammonium and

chloride species contributed the rest of this mass, with the largest contributions from

sulphate and ammonium. Sulphate contributions were very significant during the

coastal period, contributing up to 32% of the total mass. Although chlorides contributed

the least to the total mass on average, during clear biomass burning events where sharp

increases in CO and organics were observed, chlorides made up the largest component

of inorganic aerosol. Organic carbon made up approximately 80% to 90% of the total

carbon (organic carbon + elemental carbon) PM_1 mass during the campaign, with the

exception of BBP3, when this dropped to 70%. Whether these observations were a

result of burn conditions or aging processes (i.e. evaporation of organic compounds

from the aerosol phase) is unclear.

4. Outcomes of SAFIRED

The overall aim of this study was to investigate the characteristics of BB emissions in the tropical savannah region of northern Australia during the early dry season. For many gaseous and aerosol species, elevated signals were observed for much of the month-long sampling period due to the high frequency of fires. Further analysis of these species can provide more insight into the impact of these fires on the regional atmosphere. Table 2 displays a summary of companion studies undertaken within the SAFIRED campaign.

Table 3 A list of currently published companion studies undertaken during SAFIRED.

Reference	Title
Winton et al., (2016)	Dry season aerosol iron solubility in tropical northern Australia
Wang et al., (2017)	Emissions of selected semivolatile organic chemicals from forest and savannah fires
Milic et al., (2017)	Biomass burning and biogenic aerosols in northern Australia during the SAFIRED campaign
Mallet et al., (2017)	Composition, size and cloud condensation nuclei activity of biomass burning aerosol from northern Australian savannah fires
Desservattaz et al., (2017)	Emission factors of trace gases and particles from tropical savanna fires in Australia

Howard et al., (2017)	Atmospheric mercury in the southern hemisphere tropics: seasonal and diurnal variations and influence of inter-hemispheric transport

618

4.1. Emission factors and gaseous species loadings

619

620 Desservettaz et al. (2017) identified individual plumes with high signals during

621 SAFIRED in order to determine emissions factors CO_2, CO, CH_4. N_2O, as well as GEM,

622 Aitken and Accumulation mode aerosols and submicron non-refractory particle species

623 (organics, sulfates, nitrates, ammonium and chlorides). Seasonal emission factors for

624 the major greenhouse gases are important for national greenhouse gas inventories and

625 in understanding the impact of savannah fires. Furthermore, these results will be the

626 first set of emission factors for aerosol particles from savannah fires in Australia, with

627 early results suggesting higher factors than those observed from African and South

628 American savannah fires. Emission factors were mostly found to be dependent on the

629 combustion conditions (using the modified combustion efficiency as a proxy) of the

630 fires.

631

632 Wang et al. (2017) investigated 13 major PAH compounds in both the gaseous and

633 aerosol phase during the SAFIRED campaign and estimated their emission factors from

634 savannah fires, as well as for subtropical eucalypt forest fires. Concentrations of these

635 PAHs varied from from ~ 1 to over 15 ng m^{-3} within different BB periods and the

636 emission factor for savannah fires for $\sum_{13}$ PAHs were estimated to be 1600 ± 110 μg

637 kg^{-1} In the gas phase, 3- and 4-ring compounds typically contributed ~ 90% to the sum

638 concentrations whereas the particle-associated PAHs were dominated by 5- and 6-ring

639 compounds (> 80%). Measured PAH concentrations were significantly higher during

640   BBP2 and BBP4. During these periods, concentrations of BaP exceeded the monitoring

641   investigation level for atmospheric BaP (0.30 ng m^{-3}) in Australia (National-

642   Environment-Protection-Council-Service-Corporation, 2011) by up to 200%.

643

644   Biomass burning produces significant amounts of semi-volatile NMOC which can be

645   difficult to quantify and identify with current measurement techniques. However recent

646   studies have shown that including semi volatile NMOC chemistry in models improves

647   the agreement between the modeled and observed organic aerosol (Alvarado et al.,

648   2015; Konovalov et al., 2015) and ozone (Alvarado et al., 2015). High quality NMOC

649   emission factors are crucial for models to assess the impact of biomass burning plumes

650   on air quality and climate. Future analyses will be undertaken on the SAFIRED data to

651   quantify emission factors for various NMOCs.

652

653   SAFIRED represents the first measurements of atmospheric mercury undertaken in the

654   tropical region of the Australian continent. The mean observed GEM concentration

655   over the study period was 0.99 ± 0.09 ng m^{-3}, similar to the average over that month

656   (0.96 ng m^{-3}) for 5 other Southern Hemisphere sites and slightly lower than the average

657   (1.15 ng m^{-3}) for 5 tropical sites (Sprovieri et al., 2016). Mean GOM and PBM

658   concentrations were 11 ± 5 pg m^{-3} and 6 ± 3 pg m^{-3} respectively, representing 0.6 –

659   3.4% of total observed atmospheric mercury. During periods of pronounced trace gas

660   and aerosol concentrations during the campaign, spikes in GEM concentrations were

661   also observed, though there were no significant increases in GOM or PBM. Emission

662   ratios calculated during the campaign were two orders of magnitude higher than those

663   reported by Andreae and Merlet (2001). Future outcomes from the SAFIRED campaign

664   will focus on the use of micrometeorological techniques and the passive tracer radon to

665 quantify delivery of atmospheric mercury to tropical savannah ecosystems. ATARS

666 also now serves as an additional site measuring continuous GEM as part of the Global

667 Mercury Observation System (GMOS), one of only two tropical observing sites in the

668 Eastern Hemisphere and the third such site located in Australia. A discussion of the

669 seasonal and diurnal variations of atmospheric mercury at the ATARS site can be found

670 in Howard et al. (2017).

671 **4.2. Biomass burning aerosol chemistry**

672 Milic et al., (2017) provided further analysis into the aerosol chemical composition to

673 elucidate the aging of early dry season biomass burning emissions. Fractional analysis

674 (e.g., f44 and f60, the fraction of m/z 44 and m/z 60 to all organic masses, indicated

675 oxygenation and BB sources, respectively) and factor analysis using positive matrix

676 factorisation (PMF) of cToF-AMS data was investigated over the entire sampling

677 period. Outside of the periods of significant influence from BB events, three PMF-

678 resolved organic aerosol factors were identified. A BB organic aerosol factor was found

679 to comprise 24% of the submicron non-refractory organic mass, with an oxygenated

680 organic aerosol factor and a biogenic isoprene-related secondary organic aerosol factor

681 comprising 47% and 29%, respectively. These results indicate the significant influence

682 of fresh and aged BB on aerosol composition in the early dry season. The emission of

683 precursors from fires is likely responsible for some of the SOA formation.

684

685 The water uptake of aerosols during SAFIRED was further investigated in Mallet et al.,

686 (2017) to identify the influence of early dry season BB in this region on cloud

687 formation. The concentrations of cloud condensation nuclei at a constant

688 supersaturation of 0.5% were typically of the order of 2000 cm^{-3} and reached well over

689 10000 cm^{-3} during intense BB events. Variations in the ratio of aerosol particles

690 activating cloud droplets showed a distinct diurnal trend, with an activation ratio of

691 40% ± 20% during the night and 60% ± 20% during the day. The particle size

692 distribution and the hygroscopicity of the particles were found to significantly influence

693 this activation ratio. Particles were generally extremely hydrophobic, particularly

694 during the night and during the BB periods shown in this paper. Modelling CCN

695 concentrations using the size distributions of aerosols and typical continental and

696 terrestrial values of hygroscopicities yielded significant over predictions of up more

697 than 200%, highlighting the need to include more regional parameterisations of aerosol

698 composition and hygroscopicity.

699

700 Furthermore the fractional solubility of aerosol iron and other trace metals during

701 SAFIRED were investigated in Winton et al., (2016). The fractional iron solubility is

702 an important variable determining iron availability for biological uptake in the ocean.

703 On a global scale, the large variability in the observed fractional iron solubility results,

704 in part, from a mixture of different aerosol sources. Estimates of fractional iron

705 solubility from fire combustion (1 - 60 %) are thought to be greater than those

706 originating from mineral dust (1 - 2%) (Chuang et al., 2005;Guieu et al., 2005;Sedwick

707 et al., 2007), and may vary in relationship to biomass and fire characteristics as well as

708 that of the underlying terrain (Paris et al., 2010;Ito, 2011). Iron associated with BB may

709 provide information with respect to BB inputs of iron to the ocean (Giglio et al.,

710 2013;e.g. Meyer et al., 2008). The ATARS provides an ideal location to further

711 investigate BB derived fractional iron solubility at the source. The results from this

712 study can be found in Winton et al. (2016) and show that soluble iron concentrations

713 from BB sources are significantly higher than those observed in Southern Ocean

714 baseline air masses from the Cape Grim Baseline Air Pollution Station, Tasmania,

715 Australia (Winton et al., 2015). Aerosol iron at SAFIRED was a mixture of fresh BB,

716 mineral dust, sea spray and industrial pollution sources. The fractional iron solubility

717 (2 - 12%) was relatively high throughout the campaign and the variability was related

718 to the mixing and enhancement of mineral dust iron solubility with BB species.

719 ## 5. Conclusions and looking forward

720 Biomass burning was found to significantly influence the surface atmospheric

721 composition during the 2014 early dry season in north Australia. Over 28000 fires were

722 detected via satellite retrieval during the sampling period. Several periods were

723 identified when fires within 20 km of the research station resulted in significant

724 enhancements of greenhouse gases, non-methane gaseous organic compounds, gaseous

725 elemental mercury and polycyclic aromatic hydrocarbons and aerosol loadings. Much

726 of the PM_1 mass was comprised of organic material. The aerosol particle number size

727 distributions were typically unimodal and centered around 100 nm which is smaller

728 than BBA observed in other regions. The analysis of the time series of these measured

729 quantities has so far allowed the quantification of savannah fire emission factors for

730 these aerosol and gaseous species and has provided and understanding of the aerosol

731 aging, water uptake and solubility in this region.

732

733 While the specific outcomes of the SAFIRED campaign are reviewed in the previous

734 section, the general importance of this study can be discussed in a greater context. This

735 is the first large-scale collaborative project undertaken in this region and draws on the

736 resources and expertise of most of Australia's research institutes focused on atmosphere

737 chemistry and composition. Large scale, multidisciplinary measurement campaigns in

738 the tropics, such as SAFIRED, are needed to make distinctions between different types

739   of fires in different regions to reduce uncertainties in global climate models (Keywood

740   et al., 2013). This need has been recognized with the formation of global collaborative

741   initiatives promoting interdisciplinary collaboration in biomass burning research

742   (Kaiser and Keywood, 2015). As the world moves towards a warmer climate, it is

743   plausible that the frequency and intensity of biomass burning will increase, and these

744   emissions will become an increasingly important source of trace gases and aerosols to

745   the atmosphere.

746

747   SAFIRED lays the foundation for future measurements at ATARS that could make

748   measurements throughout the whole dry season and on a more long-term scale. Future

749   work in this region should focus on 1) the detailed characterisation of individual fires

750   and their emissions, 2) biomass burning emissions throughout the late dry season and

751   3) the vertical and horizontal transport of biomass burning emissions in this region.

752   With well-established emission factors, a concentrated effort should be made to link

753   modelled aerosol gaseous and aerosol loadings with *in situ* and remote sensing

754   measurements. This should be done not just at the surface, but throughout the boundary

755   layer as well as over the waters north of Australia. Furthermore, a further investigation

756   of the radiative influence of the gaseous and aerosol species should be done for this

757   region.

758   **Data availability**

759   All data are available upon request from the corresponding authors (Branka Miljevic,

760   b.miljevic@qut.edu.au; Melita D. Keywood; melita.keywood@csiro.au).

Author Contributions

M.D. Mallet[a,b,c,d,e], M.J. Desservettaz[b,c,d,e], B. Miljevic[b,c,e*], A. Milic[b,d,e], Z.D. Ristovski[b,e], J. Alroe[b,c,e], L.T. Cravigan[b,c,e], E.R. Jayaratne[d,e], C. Paton-Walsh[b,c,e], D.W.T. Griffith[b,d,e], S.R. Wilson[b,d,e], G. Kettlewell[b,e], M.V. van der Schoot[b,e], P. Selleck[b,c,d,e], F. Reisen[b,c,e], S.J. Lawson[b,c,d,e], J. Ward[b,c,d,e], J. Harnwell[b,c,e], M. Cheng[b,c,d,e], R.W. Gillett[b,c,d,e], S.B. Molloy[d,e], D. Howard[b,c,d,e], P.F. Nelson[b,e], A.L Morrison[b,e], G.C. Edwards[b,c,e], A.G. Williams[b,c,e], S.D. Chambers[b,c,d,e], S. Werczynski[b,c,e], L.R. Williams[c,d,e], V.H.L. Winton[b,c,d,e], and B. Atkinson[b,c], X. Wang[b,d,e], M.D. Keywood[b,c,d,e,f*]

a: Wrote and organised the manuscript

b: Contributed to the organisation of the campaign

c: Installed and/or operated instrumentation during the sampling period

d: Analysed data

e: Contributed to the manuscript and/or data interpretation

f: Designed and led the campaign.

*: Corresponding author

Competing interests

The authors declare that they have no conflict of interest.

Acknowledgements

40

6. References

786   Akagi, S. K., Craven, J. S., Taylor, J. W., McMeeking, G. R., Yokelson, R. J., Burling,
787   I. R., Urbanski, S. P., Wold, C. E., Seinfeld, J. H., Coe, H., Alvarado, M. J., and Weise,
788   D. R.: Evolution of trace gases and particles emitted by a chaparral fire in California,
789   Atmospheric Chemistry and Physics, 12, 1397-1421, 2012.
790   Andersen, A. N., Cook, G. D., Corbett, L. K., Douglas, M. M., Eager, R. W., Russell-
791   Smith, J., Setterfield, S. A., Williams, R. J., and Woinarski, J. C.: Fire frequency and
792   biodiversity conservation in Australian tropical savannas: implications from the
793   Kapalga fire experiment, Austral Ecology, 30, 155-167, 2005.
794   Bindoff, N. L., Stott, P. A., AchutaRao, K. M., Allen, M. R., Gillett, N., Gutzler, D.,
795   Hansingo, K., Hegerl, G., Hu, Y., Jain, S., Mokhov, I. I., Overland, J., Perlwitz, J.,
796   Sebbari, R., and Zhang, X.: Detection and Attribution of Climate Change: from Global
797   to Regional, in: Climate Change 2013: The Physical Science Basis. Contribution of
798   Working Group I to the Fifth Assessment Report of the Intergovernmental Panel on
799   Climate Change, edited by: Stocker, T. F., Qin, D., Plattner, G.-K., Tignor, M., Allen,
800   S. K., Boschung, J., Nauels, A., Xia, Y., Bex, V., and Midgley, P. M., Cambridge
801   University Press, Cambridge, United Kingdom and New York, NY, USA, 867–952,
802   2013.
803   Chambers, S. D., Hong, S.-B., Williams, A. G., Crawford, J., Griffiths, A. D., and Park,
804   S.-J.: Characterising terrestrial influences on Antarctic air masses using Radon-222
805   measurements at King George Island, Atmospheric Chemistry and Physics, 14, 9903-
806   9916, 2014.
807   Chow, J. C., Watson, J. G., Chen, L. W. A., Chang, M. C. O., Robinson, N. F., Trimble,
808   D., and Kohl, S.: The IMPROVE-A temperature protocol for thermal/optical carbon
809   analysis: maintaining consistency with a long-term database, Journal of the Air &
810   Waste Management Association, 57, 1014-1023, 2007a.
811   Chow, J. C., Watson, J. G., Chen, L. W. A., Chang, M. O., Robinson, N. F., Trimble,
812   D., and Kohl, S.: The IMPROVE-A temperature protocol for thermal/optical carbon
813   analysis: maintaining consistency with a long-term database, Journal of the Air &
814   Waste Management Association, 57, 1014-1023, 2007b.
815   Chuang, P. Y., Duvall, R. M., Shafer, M. M., and Schauer, J. J.: The origin of water
816   soluble particulate iron in the Asian atmospheric outflow, Geophysical Research
817   Letters, 32, L07813, 2005.
818   Crutzen, P. J., and Andreae, M. O.: Biomass burning in the tropics: Impact on
819   atmospheric chemistry and biogeochemical cycles, Science, 250, 1669-1678, 1990.
820   Desservettaz, M., Paton-Walsh, C., Griffith, D. W., Kettlewell, G., Keywood, M. D.,
821   Vanderschoot, M. V., Ward, J., Mallet, M. D., Milic, A., and Miljevic, B.: Emission
822   factors of trace gases and particles from tropical savanna fires in Australia, Journal of
823   Geophysical Research: Atmospheres, 2017.
824   Draxler, R. R., and Rolph, G.: HYSPLIT (HYbrid Single-Particle Lagrangian
825   Integrated Trajectory) model access via NOAA ARL READY website (http://www/.

826 arl. noaa. gov/ready/hysplit4. html). NOAA Air Resources Laboratory, Silver Spring,
827 in, Md, 2003.
828 Du, H., Kong, L., Cheng, T., Chen, J., Du, J., Li, L., Xia, X., Leng, C., and Huang, G.:
829 Insights into summertime haze pollution events over Shanghai based on online water-
830 soluble ionic composition of aerosols, Atmospheric Environment, 45, 5131-5137, 2011.
831 Dunne, E., Galbally, I. E., Cheng, M., Selleck, P., Molloy, S. B., and Lawson, S. J.:
832 Comparison of VOC measurements made by PTR-MS, Adsorbent Tube/GC-FID-MS
833 and DNPH-derivatization/HPLC during the Sydney Particle Study, 2012: a contribution
834 to the assessment of uncertainty in current atmospheric VOC measurements, Atmos.
835 Meas. Tech. Discuss, 2017, 1-24, 2017.
836 Edwards, G. C., Rasmussen, P. E., Schroeder, W. H., Wallace, D. M., Halfpenny-
837 Mitchell, L., Dias, G. M., Kemp, R. J., and Ausma, S.: Development and evaluation of
838 a sampling system to determine gaseous Mercury fluxes using an aerodynamic
839 micrometeorological gradient method, Journal of Geophysical Research: Atmospheres,
840 110, 2005.
841 Ferek, R. J., Reid, J. S., Hobbs, P. V., Blake, D. R., and Liousse, C.: Emission factors
842 of hydrocarbons, halocarbons, trace gases and particles from biomass burning in Brazil,
843 Journal of Geophysical Research, 103, 107-132, 1998.
844 Giglio, L., Randerson, J. T., and Werf, G. R.: Analysis of daily, monthly, and annual
845 burned area using the fourth-generation global fire emissions database (GFED4),
846 Journal of Geophysical Research: Biogeosciences, 118, 317-328, 2013.
847 Govender, N., Trollope, W. S., and Van Wilgen, B. W.: The effect of fire season, fire
848 frequency, rainfall and management on fire intensity in savanna vegetation in South
849 Africa, Journal of Applied Ecology, 43, 748-758, 2006.
850 Griffith, D. W. T.: Synthetic calibration and quantitative analysis of gas-phase FT-IR
851 spectra, Applied Spectroscopy, 50, 59-70, 1996.
852 Griffith, D. W. T., Deutscher, N. M., Caldow, C., Kettlewell, G., Riggenbach, M., and
853 Hammer, S.: A Fourier transform infrared trace gas and isotope analyser for
854 atmospheric applications, Atmos. Meas. Tech., 5, 2481-2498, 2012.
855 Guieu, C., Bonnet, S., Wagener, T., and Loÿe-Pilot, M. D.: Biomass burning as a source
856 of dissolved iron to the open ocean?, Geophysical Research Letters, 32, 2005.
857 Gustin, M. S., Lindberg, S. E., and Weisberg, P. J.: An update on the natural sources
858 and sinks of atmospheric mercury, Applied Geochemistry, 23, 482-493, 2008.
859 Honninger, G., von Friedeburg, C., and Platt, U.: Multi axis differential optical
860 absorption spectroscopy (MAX-DOAS), Atmospheric Chemistry and Physics, 4, 231-
861 254, 2004.
862 Howard, D., Nelson, P. F., Edwards, G. C., Morrison, A. L., Fisher, J. A., Ward, J.,
863 Harnwell, J., van der Schoot, M., Atkinson, B., Chambers, S. D., Griffiths, A. D.,
864 Werczynski, S., and Williams, A. G.: Atmospheric mercury in the southern hemisphere
865 tropics: seasonal and diurnal variations and influence of inter-hemispheric transport,
866 Atmos. Chem. Phys. Discuss., 2017, 1-20, 10.5194/acp-2017-307, 2017.
867 Iinuma, Y., Engling, G., Puxbaum, H., and Herrmann, H.: A highly resolved anion-
868 exchange chromatographic method for determination of saccharidic tracers for biomass
869 combustion and primary bio-particles in atmospheric aerosol, Atmospheric
870 Environment, 43, 1367-1371, 2009.
871 Ito, A.: Mega fire emissions in Siberia: potential supply of bioavailable iron from
872 forests to the ocean, Biogeosciences, 8, 1679-1697, 2011.
873 Jacobson, M. Z.: Strong radiative heating due to the mixing state of black carbon in
874 atmospheric aerosols, Nature, 409, 695-697, 2001.

Kaiser, J. W., and Keywood, M.: Preface for Atmos. Env. Special issue on IBBI, Atmospheric Environment, 121, 1-3, 2015.

Keil, A., and Haywood, J. M.: Solar radiative forcing by biomass burning aerosol particles during SAFARI 2000: A case study based on measured aerosol and cloud properties, Journal of Geophysical Research: Atmospheres, 108, 2003.

Keywood, M., Kanakidou, M., Stohl, A., Dentener, F., Grassi, G., Meyer, C. P., Torseth, K., Edwards, D., Thompson, A. M., Lohmann, U., and Burrows, J.: Fire in the air: Biomass burning impacts in a changing climate, Critical Reviews in Environmental Science and Technology, 43, 40-83, 2013.

Landis, M. S., Stevens, R. K., Schaedlich, F., and Prestbo, E. M.: Development and characterization of an annular denuder methodology for the measurement of divalent inorganic reactive gaseous mercury in ambient air, Environmental science & technology, 36, 3000-3009, 2002.

LaRoche, J., and Breitbarth, E.: Importance of the diazotrophs as a source of new nitrogen in the ocean, Journal of Sea Research, 53, 67-91, 2005.

Lawson, S. J., Keywood, M. D., Galbally, I. E., Gras, J. L., Cainey, J. M., Cope, M. E., Krummel, P. B., Fraser, P. J., Steele, L. P., Bentley, S. T., Meyer, C. P., Ristovski, Z., and Goldstein, A. H.: Biomass burning emissions of trace gases and particles in marine air at Cape Grim, Tasmania, Atmospheric Chemistry and Physics, 15, 13393-13411, 2015.

Lin, N.-H., Tsay, S.-C., Maring, H. B., Yen, M.-C., Sheu, G.-R., Wang, S.-H., Chi, K. H., Chuang, M.-T., Ou-Yang, C.-F., and Fu, J. S.: An overview of regional experiments on biomass burning aerosols and related pollutants in Southeast Asia: From BASE-ASIA and the Dongsha Experiment to 7-SEAS, Atmospheric Environment, 78, 1-19, 2013.

Liousse, C., Devaux, C., Dulac, F., and Cachier, H.: Aging of savanna biomass burning aerosols: Consequences on their optical properties, Journal of Atmospheric Chemistry, 22, 1-17, 1995.

Manninen, H. E., Petaja, T., Asmi, E., Riipinen, I., Nieminen, T., Mikkila, J., Horrak, U., Mirme, A., Mirme, S., Laakso, L., Kerminen, V. M., and Kulmala, M.: Long-term field measurements of charged and neutral clusters using Neutral cluster and Air Ion Spectrometer (NAIS), Boreal Environment Research, 14, 591-605, 2009.

Meyer, C., Cook, G., Reisen, F., Smith, T., Tattaris, M., Russell-Smith, J., Maier, S., Yates, C., and Wooster, M.: Direct measurements of the seasonality of emission factors from savanna fires in northern Australia, Journal of Geophysical Research: Atmospheres (1984–2012), 117, 2012.

Meyer, C. P., Luhar, A. K., and Mitchell, R. M.: Biomass burning emissions over northern Australia constrained by aerosol measurements: I—Modelling the distribution of hourly emissions, Atmospheric Environment, 42, 1629-1646, 2008.

Mirme, A., Tamm, E., Mordas, G., Vana, M., Uin, J., Mirme, S., Bernotas, T., Laakso, L., Hirsikko, A., and Kulmala, M.: A wide-range multi-channel Air Ion Spectrometer, Boreal Environmental Research, 12, 247-264, 2007.

National-Environment-Protection-Council-Service-Corporation: National Environment Protection (Air Toxics) Measure, 2011.

Paris, R., Desboeufs, K., Formenti, P., Nava, S., and Chou, C.: Chemical characterisation of iron in dust and biomass burning aerosols during AMMA-SOP0/DABEX: implication for iron solubility, Atmospheric Chemistry and Physics, 10, 4273-4282, 2010.

Penner, J., Chuang, C., and Grant, K.: Climate forcing by carbonaceous and sulfate aerosols, Climate Dynamics, 14, 839-851, 1998.

925 Rea, A. W., Lindberg, S. E., Scherbatskoy, T., and Keeler, G. J.: Mercury accumulation
926 in foliage over time in two northern mixed-hardwood forests, Water, Air, and Soil
927 Pollution, 133(1-4), 49-67, 2002.
928 Russell-Smith, J., Yates, C. P., Whitehead, P. J., Smith, R., Craig, R., Allan, G. E.,
929 Thackway, R., Frakes, I., Cridland, S., Meyer, M. C. P., and Gill, M.: Bushfires' down
930 under': patterns and implications of contemporary Australian landscape burning,
931 International Journal of Wildland Fire, 16, 361-377, 2007.
932 Russell-Smith, J., Cook, G. D., Cooke, P. M., Edwards, A. C., Lendrum, M., Meyer,
933 C., and Whitehead, P. J.: Managing fire regimes in north Australian savannas: applying
934 Aboriginal approaches to contemporary global problems, Frontiers in Ecology and the
935 Environment, 11, e55-e63, 2013.
936 Saarikoski, S., Sillanpää, M., Sofiev, M., Timonen, H., Saarnio, K., Teinilä, K.,
937 Karppinen, A., Kukkonen, J., and Hillamo, R.: Chemical composition of aerosols
938 during a major biomass burning episode over northern Europe in spring 2006:
939 Experimental and modelling assessments, Atmospheric Environment, 41, 3577-3589,
940 2007.
941 Sedwick, P. N., Sholkovitz, E. R., and Church, T. M.: Impact of anthropogenic
942 combustion emissions on the fractional solubility of aerosol iron: Evidence from the
943 Sargasso Sea, Geochemistry, Geophysics, Geosystems, 8, 2007.
944 Shi, Y., Matsunaga, T., Saito, M., Yamaguchi, Y., and Chen, X.: Comparison of global
945 inventories of CO_2 emissions from biomass burning during 2002–2011 derived from
946 multiple satellite products, Environmental Pollution, 206, 479-487, 2015.
947 Singh, H., Brune, W., Crawford, J., Jacob, D. J., and Russell, P.: Overview of the
948 summer 2004 Intercontinental Chemical Transport Experiment–North America
949 (INTEX-A), Journal of Geophysical Research: Atmospheres, 111, 2006.
950 Sinreich, R., Friess, U., Wagner, T., and Platt, U.: Multi axis differential optical
951 absorption spectroscopy (MAX-DOAS) of gas and aerosol distributions, Faraday
952 Discuss, 130, 153-164, 2005.
953 Sprovieri, F., Pirrone, N., Bencardino, M., D'Amore, F., Carbone, F., Cinnirella, S.,
954 Mannarino, V., Landis, M., Ebinghaus, R., Weigelt, A., Brunke, E. G., Labuschagne,
955 C., Martin, L., Munthe, J., Wängberg, I., Artaxo, P., Morais, F., Cairns, W., Barbante,
956 C., Diéguez, M. D. C., Garcia, P. E., Dommergue, A., Angot, H., Magand, O., Skov,
957 H., Horvat, M., Kotnik, J., Read, K. A., Neves, L. M., Gawlik, B. M., Sena, F.,
958 Mashyanov, N., Obolkin, V. A., Wip, D., Feng, X. B., Zhang, H., Fu, X.,
959 Ramachandran, R., Cossa, D., Knoery, J., Marusczak, N., Nerentorp, M., and Norstrom,
960 C.: Atmospheric Mercury Concentrations observed at ground-based monitoring sites
961 globally distributed in the framework of the GMOS network, Atmospheric Chemistry
962 and Physics Discussions, 2016, 1-32, 2016.
963 Steffen, A., Douglas, T., Amyot, M., Ariya, P., Aspmo, K., Berg, T., Bottenheim, J.,
964 Brooks, S., Cobbett, F., Dastoor, A., Dommergue, A., Ebinghaus, R., Ferrari, C.,
965 Gardfeldt, K., Goodsite, M. E., Lean, D., Poulain, A. J., Scherz, C., Skov, H., Sommar,
966 J., and Temme, C.: A synthesis of atmospheric mercury depletion event chemistry in
967 the atmosphere and snow, Atmospheric Chemistry and Physics, 8, 1445-1482, 2008.
968 Stockwell, C., Yokelson, R., Kreidenweis, S., Robinson, A., DeMott, P., Sullivan, R.,
969 Reardon, J., Ryan, K., Griffith, D., and Stevens, L.: Trace gas emissions from
970 combustion of peat, crop residue, domestic biofuels, grasses, and other fuels:
971 configuration and Fourier transform infrared (FTIR) component of the fourth Fire Lab
972 at Missoula Experiment (FLAME-4), Atmospheric Chemistry and Physics, 9727, 2014.

973 Tuch, T. M., Haudek, A., Müller, T., Nowak, A., Wex, H., and Wiedensohler, A.:
974 Design and performance of an automatic regenerating adsorption aerosol dryer for
975 continuous operation at monitoring sites, Atmos. Meas. Tech., 2, 417-422, 2009.

976 van der Werf, G. R., Randerson, J. T., Giglio, L., Collatz, G., Mu, M., Kasibhatla, P.
977 S., Morton, D. C., DeFries, R., Jin, Y. v., and van Leeuwen, T. T.: Global fire emissions
978 and the contribution of deforestation, savanna, forest, agricultural, and peat fires (1997–
979 2009), Atmospheric Chemistry and Physics, 10, 11707-11735, 2010.

980 Wang, X., Thai, P. K., Mallet, M., Desservettaz, M., Hawker, D. W., Keywood, M.,
981 Miljevic, B., Paton-Walsh, C., Gallen, M., and Mueller, J. F.: Emissions of selected
982 semivolatile organic chemicals from forest and savannah fires, Environmental science
983 & technology, 51, 1293-1302, 2017.

984 Whittlestone, S., and Zahorowski, W.: Baseline radon detectors for shipboard use:
985 Development and deployment in the First Aerosol Characterization Experiment (ACE
986 1), Journal of Geophysical Research: Atmospheres, 103, 16743-16751, 1998.

987 Winton, V., Bowie, A., Edwards, R., Keywood, M., Townsend, A., van der Merwe, P.,
988 and Bollhöfer, A.: Fractional iron solubility of atmospheric iron inputs to the Southern
989 Ocean, Marine Chemistry, 177, 20-32, 2015.

990 Winton, V., Edwards, R., Bowie, A., Keywood, M., Williams, A., Chambers, S.,
991 Selleck, P., Desservettaz, M., Mallet, M., and Paton-Walsh, C.: Dry season aerosol iron
992 solubility in tropical northern Australia, Atmospheric Chemistry and Physics
993 Discussions, doi:10.5194/acp-2016-419, 2016.

994 Wong, J., and Li, Z.: Retrieval of optical depth for heavy smoke aerosol plumes:
995 uncertainties and sensitivities to the optical properties, Journal of the Atmospheric
996 Sciences, 59, 250-261, 2002.

997 Yokelson, R. J., Crounse, J. D., DeCarlo, P. F., Karl, T., Urbanski, S., Atlas, E.,
998 Campos, T., Shinozuka, Y., Kapustin, V., Clarke, A. D., Weinheimer, A., Knapp, D. J.,
999 Montzka, D. D., Holloway, J., Weibring, P., Flocke, F., Zheng, W., Toohey, D.,
1000 Wennberg, P. O., Wiedinmyer, C., Mauldin, L., Fried, A., Richter, D., Walega, J.,
1001 Jimenez, J. L., Adachi, K., Buseck, P. R., Hall, S. R., and Shetter, R.: Emissions from
1002 biomass burning in the Yucatan, Atmospheric Chemistry and Physics, 9, 5785-5812,
1003 2009.

1004

1005

1006